Otology & Neurotology
35:686–694 © 2014, Otology & Neurotology, Inc.

The Inner Structure of Human Otoconia

*Leif Erik Walther, †Alexander Blödow, †Marc Boris Bloching, ‡Jana Buder, ‡Wilder Carrillo-Cabrera, ‡Elena Roseeva, ‡Horst Borrmann, ‡Paul Simon, and ‡Rüdiger Kniep

**Department of Otorhinolaryngology, Head and Neck Surgery, University Medicine Mannheim, Ruprecht-Karls University Heidelberg, Germany; †Department of Otorhinolaryngology, Helios Clinic Berlin-Buch, Berlin, Germany; and ‡Max Planck Institute for Chemical Physics of Solids, Dresden, Germany*

Background: The architecture of human otoconia has been only poorly understood up to now. Currently, it is assumed that otoconia contain a central core surrounded by a shell.
Objectives: To investigate the inner structure of human otoconia.
Methods: Human otoconia were investigated by environmental scanning electron microscopy (ESEM). The diffraction behavior was analyzed using X-ray techniques (XRD). Focused ion beam (FIB) slices of otoconia were investigated by transmission electron microscopy (TEM). The results were correlated with observations on degenerate human otoconia and decalcification experiments using ethylenediaminetetraacetic acid (EDTA). Artificial otoconia (calcite-gelatine and calcite-gelatine/agarose composites) were investigated in the same way and compared with human otoconia.
Results: Human otoconia represent highly mosaic-controlled calcite-based nanocomposites. The inner structure is composed of 3 + 3 branches with an ordered arrangement of nanocomposite particles and parallel orientation of fibrils. The surrounding belly is less ordered and appears more porous. Degenerate otoconia show a successive dissolution of the belly region exposing to the inner structure (branches) in later stages of degeneration. Artificial otoconia reveal identical chemical, crystallographic and morphologic patterns. They are, however, larger in size.
Conclusion: Human otoconia show an inner architecture consisting of a less dense belly region and 3 + 3 more dense branches meeting at a central point (center of symmetry). The differences in volume densities and the resulting solubility may play a role in BPPV. Artificial otoconia may serve as a model for further investigations.
Key Words: Benign paroxysmal positional vertigo—Cervical vestibular evoked myogenic potential—Ocular vestibular evoked myogenic potential—Otoconia—Otolith organs—Saccule—Utricle.
Otol Neurotol **35:**686–694, 2014.

Otoconia represent essential functional components of the otolith organs located on top of the sensory epithelium of the utricle and the saccule (1). Because of their inertial mass, otoconia provide the mechanical stimulus, which leads to a deflection of vestibular hair cells to enable the otolith system to detect linear accelerations and head tilts relative to the gravity vector, which is the reference in space (2).

Up to now, there have been various investigations on the composition, diffraction behavior and architecture of human otoconia; however, there are significant discrepancies in the interpretation of the inner structure (3–13). The current common assumption is that otoconia are composed of a central core surrounded by an outer shell (11–13).

The aim of this study was to definitely resolve the inner structure of human otoconia. Starting from investigations on the outer shape and chemical composition, we used a precise cutting procedure (focused ion beam, FIB) to finally derive a 3D picture. Based on earlier investigations on calcite–gelatine and calcite gelatine/argarose composites (CGC, CGAC) in vitro, it was already concluded that even the inner structure should show close relations to vital human otoconia (14–16). Hence, the artificial otoconia may serve as a model for further investigations.

MATERIALS AND METHODS

Specimen and Structural Investigations

Vital human utricular otoconia were extracted in patients undergoing transmastoid labyrinthectomy. Specimens of intact and degenerate otoconia were identified using environmental scanning electron microscopy (ESEM, FEI Quanta 200 FEGi; Eindhoven, The Netherlands) in low vacuum (LV, 60 Pa) and high vacuum (HV, 2×10^{-4} Pa) modes. A backscatter and a secondary electron detector were used to detect contrast differences.

X-ray Cristallography and Chemical Composition

For single crystal X-ray diffraction experiments, a single intact human otoconium was glued on a glass capillary (Fig. 1).

Address correspondence and reprint requests to Leif Erik Walther, M.D., Ph.D., University Medicine Mannheim, Ruprecht-Karls University Heidelberg, Theodor-Kutzer-Ufer 1-3 D-68167, Mannheim, Germany; E-mail: Leif.Walther@hno-praxis-sulzbach.de
The authors disclose no conflicts of interest.

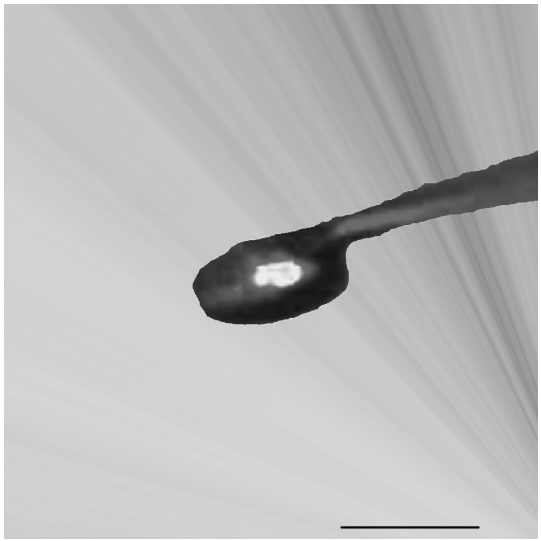

FIG. 1. For X-ray single crystal diffraction experiments a single human otoconium (optical micrograph) is glued on a glass capillary (scale bar = 5 μm).

Diffraction data were collected on a Rigaku R-AXIS SPIDER diffractometer using Ag-*Kα* radiation (0.56087 Å).

By use of the Bragg-part of the diffraction pattern (reflections strictly based on the Bragg equation), the crystal structure of calcite could be solved (15) without evidence for the presence of the organic component, which, however, is a real part of the composite structure of otoconia.

The pattern of the organic component is observed by TEM (see below). In fact, otoconia represent a highly mosaic-controlled nanosuperstructure by taking into account the distribution of the organic molecules within the calcite matrix.

The amount of the organic component of vital human otoconia and artificial otoconia was analyzed as described recently (14,15).

FIB Preparation and TEM Investigations

Intact human otoconia were selected from the specimen with a micromanipulator and attached on top of a FIB holder (Figs. 4A and 5A). The desired region for FIB cutting of otoconia was covered with a platinum (Pt) mask (thickness 1–2 μm, acceleration voltage 30 kV, current 0.3 nA) (Figs. 4A and 4B). Several otoconia were sliced longitudinally and crosswise in different planes to reach electron transparency (thickness of 50–100 nm, 30 kV acceleration voltages, HV, currents of 3–0.05 nA for the Ga^+-beam) on an FEI Quanta™ 200 3Di DualBeam device (FEI company, Eindhoven, The Netherlands) (Figs. 4C and 5C).

Decalcification

For decalcification, intact human otoconia were treated with ethylenediaminetetraacetic acid (EDTA, c = 0.001–0.0025 mol/l). The morphologic changes were investigated using ESEM (2-min steps).

Artificial Otoconia

Artificial otoconia (CGC and CGAC) were produced in vitro by use of the double diffusion technique in a protein matrix (gelatin and gelatin/agarose) (14,15). The morphogenesis of CGC and CGAT was observed by ESEM. Further characterization was performed according to the procedures used for human otoconia.

Ethics

The study was conducted in conformity with the declaration of Helsinki and approved by the ethics committee of the University Medicine Mannheim (2012-612N-MA).

RESULTS

Outer Morphology of Intact and Degenerate Human Otoconia

Intact human otoconia consist of a cylindrical body with 3 rhombohedral faces at both ends. The cross section of the cylindrical body is shaped in a roughly hexagonal outline. The body region contains numerous pores with decreasing size in direction to the terminal faces. The surface of the body is randomly roughened, whereas the rhombohedral faces are more structured, indicating the presence of a composite nanostructure. The terminal faces at both ends are turned by 60 degrees toward each other (Fig. 2A).

Degeneration of human otoconia leads to destruction of the belly area extending to the center of symmetry, whereas the branches with their rhombohedral faces remain nearly unaffected in early stages (Fig. 2B) but are involved in later stages of degeneration.

X-ray Diffraction and Chemical Composition of Intact Human Otoconia

The Bragg pattern of a single otoconium corresponds to a single crystal of calcite (the inorganic part of the composite) (Fig. 3).

The amount of organic molecules (proteins) is approximately 3.3% of their total weight.

This is a maximum value because organic material attached to the surface cannot perfectly be removed from human otoconia because they are very small in size. Because of this small size of human otoconia, samples used for analytical investigations may contain a relatively higher amount of organic material.

TEM Analyses of FIB Cuts

Otoconia consist of an ordered arrangement of organic fibrils together with calcite-based nanocrystals representing a mosaic structure. Thin FIB cuts in several planes reveal differences in the mosaic structure, which are caused by different regions showing different alignment of organic fibrils. The more dense structure shows a nearly perfect periodic calcite pattern and a parallel orientation of the integrated and mineralized protein fibrils. The packing sequence of fibrils (periodicity of about 20 nm) extends in direction to the rhombohedral faces represented by 3 + 3 branches. This dumbbell-like branch structure is surrounded by a less ordered structure (belly) consisting of nanodomains in a less ordered arrangement and of a large number of pores (Figs. 4, D–F, and 5, D–F).

The branches are turned by 60 degrees corresponding to their terminal faces.

A center of symmetry is present in the center of the otoconia (Fig. 6).

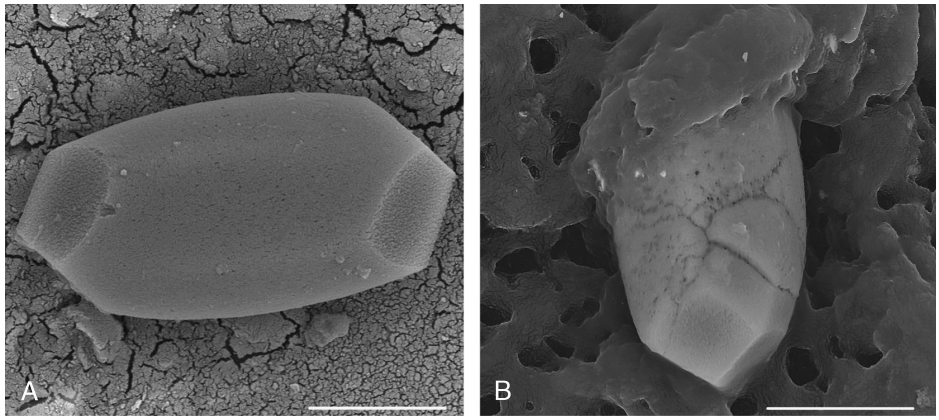

FIG. 2. *A*, Single intact vital human otoconium. The more regular surface structures of the rhombohedral faces differ significantly from the surface of the cylindrical body indicating different areas of the composite structures, (ESEM, HV, 15 kV, scale bar = 5 μm). *B*, Vital human otoconium affected by degeneration. Pores are deepened and fissures occur. The belly area is more affected than the rhombohedral faces, (ESEM, HV/Au, 15 kV, scale bar = 5 μm).

The overall X-ray diffraction pattern (Bragg pattern) of human otoconia shows a common crystallographic orientation of branch and belly areas (Fig. 3). Electron diffraction patterns are consistent with the X-ray data corresponding to calcite and indicating an overall single crystal behavior. A 3D picture of a single otoconium is modeled in Figure 7.

Decalcification

In early stages (2–6 min), EDTA treatment of otoconia leads to hole formation affecting the belly but leaving the branches nearly unaffected. In later stages (>6 min), the belly area is completely dissolved; however, the dense internal structure (branches) remains. When the inorganic component (calcite) is completely dissolved, the organic component remains and shows the initial shape of otoconia. ESEM observations with backscatter and the secondary electron detectors reveal the presence of 2 internal structures, which are different in their densities. The more dense structure consists of the trigonal branches connected by a center of symmetry. The less dense parts surround the branches and correspond to the belly region (Fig. 8).

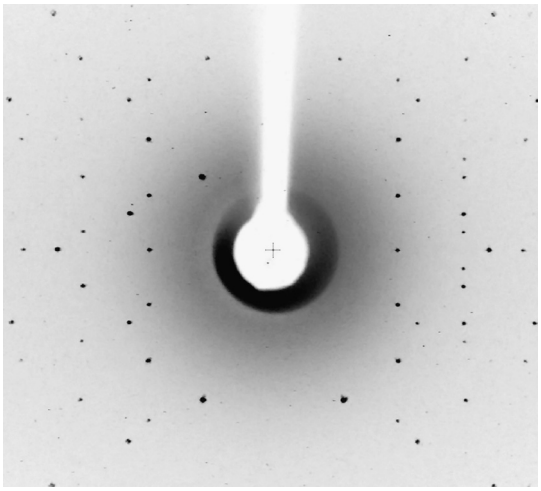

FIG. 3. X-ray diffraction pattern (Ag-$K\alpha$ radiation) of a human otoconium (Fig. 1) showing a Bragg pattern consistent with a single crystal. The crystal structure (calcite) was solved from the diffraction data (14).

Artificial Otoconia

The shape development of artificial otoconia (CGC/CGAC) is shown in Figure 9, A to D. The morphogenesis starts with gradual formation of the 6 branches and the corresponding rhombohedral faces. Nucleation obviously starts from a common region close to the center of otoconia (center of symmetry).

In immature artificial otoconia, the branches represent the highly dense internal structure acting as a backbone during shape development. The less dense belly region grows more slowly and reveals the more porous nanocomposite structure.

Maturation of artificial otoconia is completed after a few days. CGAC showed a less bulbous body than CGC. The size of CGC and CGAC is up to 500 μm. XRD patterns of CGC and CGAC showed similar results as observed for human otoconia, with the Bragg patterns (Fig. 3) being representative for a single crystal of calcite. XRD patterns of artificial otoconia are shown in references 14 and 15. The organic minority component ranges between 1.9% and 2.5% of their total weight, respectively. The composite nature of the artificial specimen is associated with a total density of 2.563 g/cm^3. FIB cuts of artificial otoconia in several orientations reveal an internal structure resembling the internal structure of human otoconia. The periodicity of the mineralized fibers within the branches is approximately 25 nm. EDTA exposure causes stepwise dissolution of calcite corresponding to the scenario observed for human otoconia (Fig. 10).

DISCUSSION

The morphologic integrity of otolith organs is a prerequisite for maintaining balance and orientation in space (1, 2).

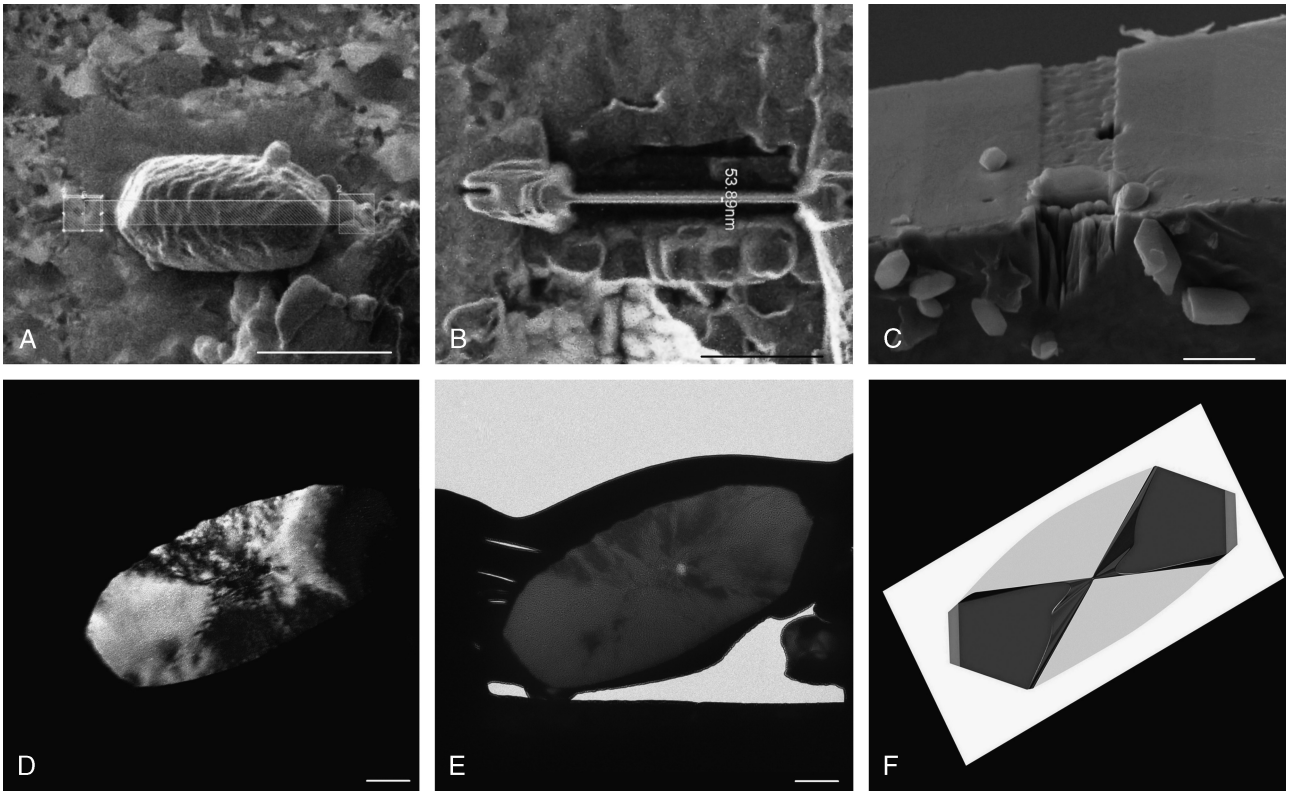

FIG. 4. *A*, For preparation of a longitudinal FIB cut a single human otoconium is placed on top of a FIB sample holder. *B*, The selected slice (marked area in *A*) is covered with a thin Pt-layer for protection before slicing and was sliced down to 50–100 nm, (scanning ion microscopy (SIM), top view, HV 30 kV, scale bar = 2 μm). *C*, Front view of the thin slice of an otoconium prepared for TEM investigations, (SEM, front view, HV, 30 kV, scale bar = 3 μm). *D* and *E*, Longitudinal slice of a single otoconium approximately through the center with different contrast modes showing differences in structured orientations and resulting in dense areas (branches) and less dense areas (belly) (dark field TEM images and bright field TEM images, respectively, TEM, scale bar = 500 nm). *F*, Corresponding model of the inner structure according to the results of TEM analyses showing branches and belly part as the underlying inner structure.

It has been shown that morphologic alterations may be present in animal and human otoconia because of degenerative processes (5,16–19). However, the observed degenerative processes do not fit the current model of otoconia morphology assuming a core/shell structure (11–13).

Based on the results of the present study, we confirm recent investigations revealing that human otoconia show a characteristic outer shape with specific symmetry properties independent of their size (14). The results of diffraction analyses revealed Bragg patterns, confirming that human otoconia behave like single crystals of calcite, characterizing them as calcite-based composites.

To investigate details of the internal structure, we used the FIB technique, which is currently applied to clarify the internal structure of solids without destruction effects (20). Our results demonstrate that also biominerals, such as human otoconia, can be precisely sliced to investigate structural details by TEM on the nanoscale (50–100 nm). The results of TEM FIB cuts in several orientations reveal an intergrowth structure of inorganic and organic components characterizing human otoconia as highly mosaic-controlled calcite-based nanocomposites. This, in general, confirms the study of Ross and Pote, who found mammalian otoconia (rats) to be mosaic biominerals, resembling a mosaic arrangement of nanocrystals (7). Recently, Andrade et al. observed in rat otoconia a hexagonal arrangement of fibrils corresponding to the properties of a mosaic nanostructure (13). In our study, however, the FIB method enables a detection of the exact arrangement of the inner architecture with different alignments of fibrils. FIB slices in several planes show a highly dense structure with 3 cones (3 + 3 branches) on each side integrating the terminal faces and a more porous, less dense structure surrounding the branches (belly).

The branches are more dense because of the highly ordered arrangement of nanocomposite units together with a parallel arrangement of fibrils. The belly area appears to be less dense caused by a less ordered nanocomposite structure together with pores. Thus, the branch and belly regions differ in their volume densities.

Both the belly and the branch parts reveal Bragg patterns like single crystals, whereas the organic components do not significantly contribute to this diffraction part. This kind of solid matter is also called a 3D periodic arrangement of nanocompartments strongly affected by defects and disorder, which is common for biominerals including otoconia. In a recent study, the Bragg pattern of ultra-thin sections (70 nm, diamond knife) of rat otoconia

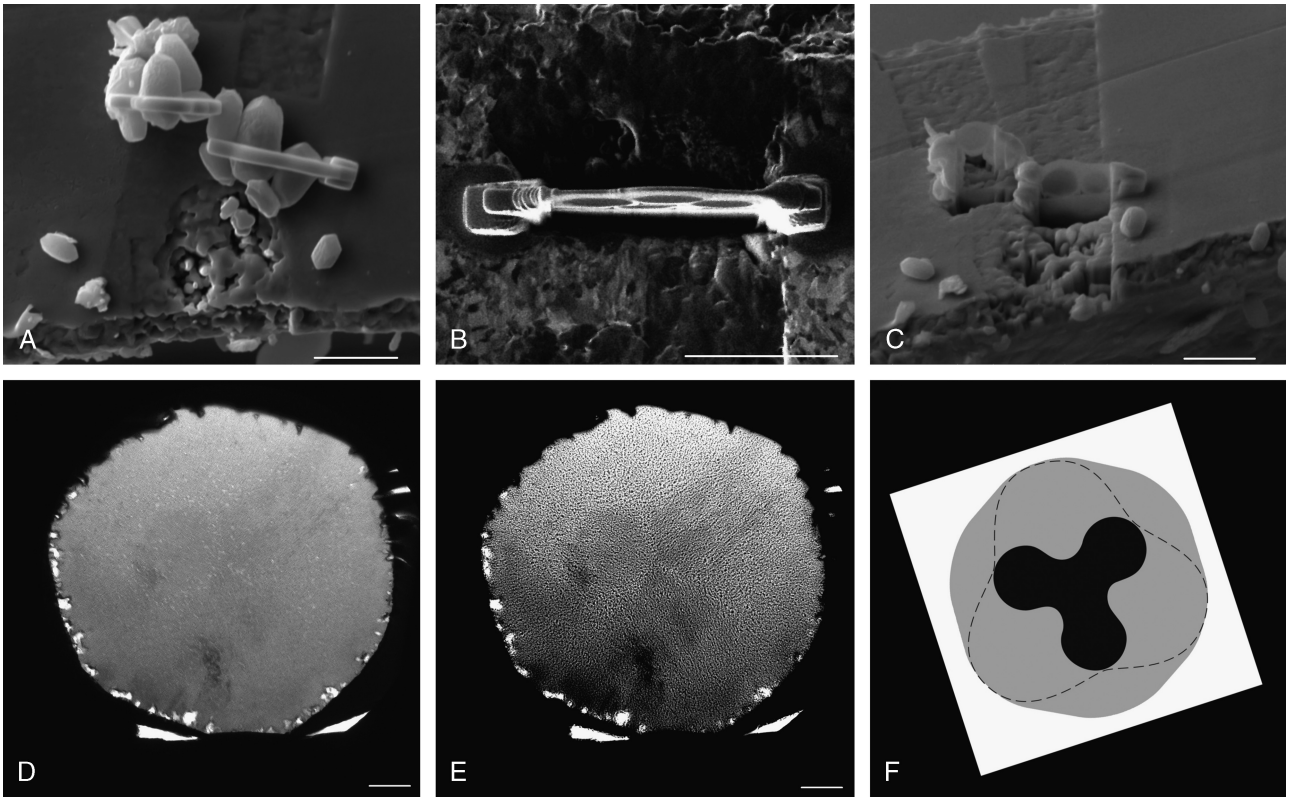

FIG. 5. *A*, Human otoconia chosen for cross-sectional FIB cuts together with platinum mask (SEM, top view, HV, 30 kV scale bar = 5 μm). *B*, Intermediate stage of a single slice during the FIB cut procedure (SIM, top view, HV, 30 kV, scale bar = 3 μm,) and (*C*) Slice surface ready for TEM analyses (SEM, front view, HV, 30 kV, scale bar = 5 μm). *D*, Bright field TEM images in focus and (*E*) Over focus of a paramedian cross sectional slice of an otoconium showing the inner structure represented by more dark regions (branches) surrounded by less dense areas (belly) (TEM, front view, scale bar = 200 nm). *F*, Planar reconstruction of the inner structure based on the paramedian FIB cut cross sections showing symmetrical branches surrounded by the belly.

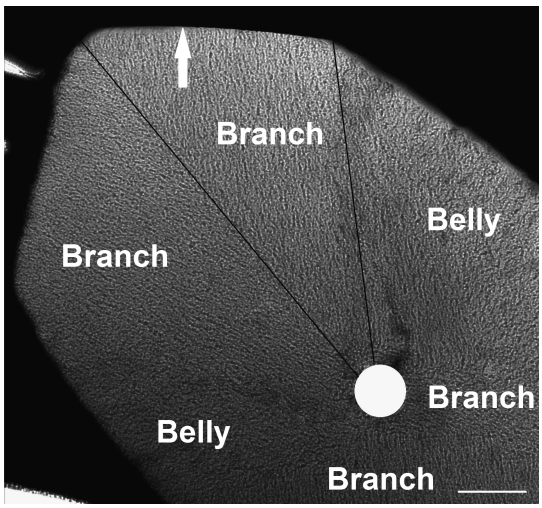

FIG. 6. *A*, Transversal FIB cut showing the branch areas of an otoconium containing fibrils in parallel arrangement. The *black lines* define one branch area. The *white arrow* shows the direction of fibrils within one branch running perpendicular to the rhombohedral endface. The *white point* corresponds to the center of symmetry of the otoconium. The belly regions appear to be less ordered (TEM, scale bar = 200 nm).

was shown. The authors also observed a sharp borderline within the inner structure of animal otoconia (mice and guinea pigs), which separates a more dense outer cortex and a less dense inner core (13). They concluded that there is a core/shell scenario as the underlying inner structure of otoconia. However, with regard to the results of Andrade et al., the densely mineralized cortex with

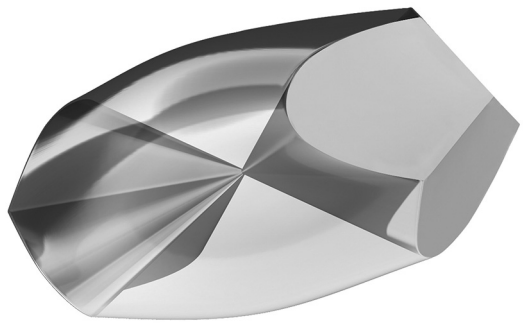

FIG. 7. Three-dimensional model of a complete otoconium. The planar rhombohedral faces define the closing planes of the branches.

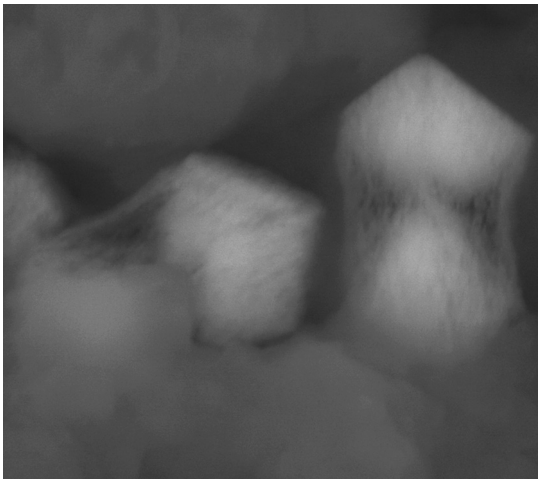

FIG. 8. Human otoconia after treatment with EDTA, observed by the use of a backscatter detector. The branches are still present. The net of fibrils within the former composite belly region interconnects the 2 parts of the remaining dumbbells containing the 3 + 3 branches. (ESEM, 15 kV, HV, scale bar = 2 μm).

parallel-arranged rows corresponds to parts of the branches, and the less dense inner core has to be considered as part of the belly (13).

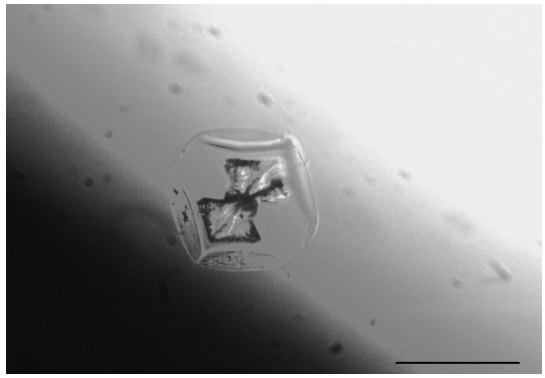

FIG. 10. Artificial (biomimetic) otoconium (CGC) after EDTA exposure. While the belly area is completely dissolved, parts of the more dense structured branches are still present. The organic component keeps the shape of the former composite (light microscope, in solution, scale bar = 100 μm).

In earlier studies, Marco et al. and Sànchez-Fernàndez et al. described ultramicrotom sections of guinea-pig otoconia containing 2 zones of different densities (Fig. 12A) (9,10). Taking the results of our study, it becomes clear that the oblique cuts show parts of the branches and the belly region (Fig. 12B). The authors also report on a parallel

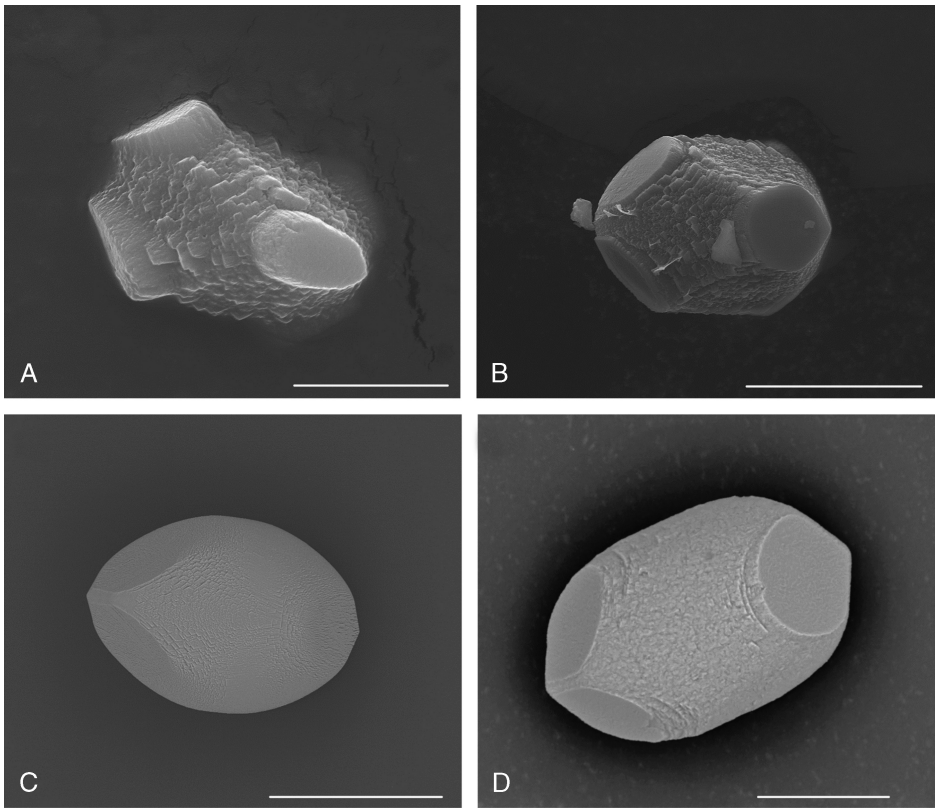

FIG. 9. *A*, Artificial (biomimetic) otoconia (CGC) reveal a gradual growth process. Early stages of the development reveal 6 branches with terminal faces at both ends (ESEM, 20 kV,HV, scale bar = 5 μm). *B*, The branches grow faster than the less ordered (less structured) belly region (ESEM, 20 kV, HV, scale bar = 20 μm). *C*, Mature CGC (ESEM, 20 kV, high vacuum, scale bar = 400 μm) *D*, and CGAC, (ESEM, 15 kV, HV, scale bar = 50 μm).

structuring in the periphery of otoconia (9,10). The results of our study show that each branch is characterized by a parallel arrangement of mineralized protein fibrils running perpendicularly to the surface of the terminal planes. This orientation in the direction of the rhombohedral faces causes the specific surface structure revealing the rhombohedral planes to represent the visible part of the dense internal architecture (branches). This specific inner architecture of otoconia also confirms the existence of a center of symmetry situated in the center of otoconia. The branches develop from this center and are turned by 60 degrees, revealing a symmetry close to -3*m*. The symbol "-3*m*" defines the point group (crystal class)-symmetry of a polyhedron by use of the so-called Hermann-Mauguin-notation. Otoconia contain a 3-fold rotation axis combined with a center of symmetry (indicated by -3) and a mirror plane containing the 3-fold rotation axis, which causes tripling of the mirror plane. The complete symbol is therefore -3*m*, which also holds for a pure calcite single crystal (e.g., a calcite cleavage rhombohedron).

Fermin et al. presented a 2-dimensional X-shaped plane model of fibrils in chicken otoconia showing an arrangement of fibrils starting from the center of otoconia assuming that this might be the "core" (8). According to the results of our study, the X-shape structure corresponds to the presence of 2 of the dense branches starting from the center of the otoconia, but it does not represent a central core.

The interpretation of fibril orientations, their size and position as well as a structure with a "central core" together with a surrounding shell differs in several publications. In crushed human otoconia, Carlström et al. found dust-like fibril structures assumed to represent an inner nucleus (3). Further investigations in rat otoconia using freeze etching techniques reported on a far-reaching, less dense central organic core formed by a tight meshwork of filaments and a dense crystalline outer shell in rats and mice (11,13). With the results of our study, we can verify that there is no core/shell structure in human otoconia as visualized in our 3D model (Fig. 6). This model reveals the inner architecture showing the 2 areas with different composite densities, the symmetry properties, and the existence of a dumbbell-like mass distribution. The latter may become of interest for explanations of the functionality of otoconia.

The results of this study and earlier observations of human otoconia confirm our results on the inner structure derived from the FIB slice investigations. Ross et al. (21) observed degenerate otoconia fragments in humans and also report on an internal, tripartite configuration in case of fragment formation which is fully consistent with the results of the present study.

In case of degeneration, the less dense structure of the belly region causes its higher susceptibility to any degenerative attack. In early stages of degeneration, it can be assumed that the pores of the belly provide access for endolymph to the internal structures of otoconia and mediate decalcification scenarios. This process can lead to a deepening of the pores until fissures occur. The less dense belly region becomes increasingly damaged, whereas the branches including the rhombohedral faces stay initially safe and less affected. This is supported by the results of EDTA exposure to otoconia.

The EDTA experiments on human otoconia also confirm the inner architecture of human otoconia showing an anisotropic solubility. In earlier stages of decalcification, a hole formation of the belly area verifies the low volume density of this region. The branches, however, with their high volume density are affected in later stages. The trigonal area of the otoconia, which is observed after EDTA treatment, corresponds to the 3 + 3 dense branches.

Based on EDTA experiments and the observation on human otoconia in earlier stages of degeneration, it can be assumed that separated nanoparticles or remnants of the belly within the endolymph may indicate the presence of otoconia degeneration as in BPPV related to the high incidence of degenerative BPPV at higher ages.

Several studies confirm that degenerative processes lead to a residue of dumbbell structures in later stages of otoconia degeneration. With progressive degeneration fragment formation is visible. With evolving degeneration scenarios, the inner architecture of otoconia causes the extension of dissolution processes to the center of symmetry of otoconia, resulting in fractures mainly through that center. This degeneration procedure leads to fragments solely composed of the 3 + 3 dense branch parts of otoconia. This scenario may explain recurrent or persistent cases of degenerative BPPV at higher ages.

The results of our study also show that the chemical and morphological patterns of CGC and CGAC are closely related to those of human otoconia differing only in size. The chance to reproduce (mimic) a biomineral in its intrinsic nanostructure and its outer shape in the laboratory opens up a wide area for further studies of morphogenesis, biomechanics, degeneration, and repair processes. Artificial otoconia might serve as a model for further investigation of vital human otoconia properties, which can only be obtained by surgical procedures.

In summary, we show that human otoconia contain a uniform structural architecture composed of 3 + 3 dense branches surrounded by a less dense belly area. Using FIB cuts and TEM, we demonstrate that the current view of a core/shell relation was caused by accidental scratches only (10,11). Furthermore, we clearly explain the reasons for this assumption using reconstructions. Our 3D model of human otoconia reveals that the specific inner architecture may produce images of different structures depending on the region and the direction of scratches or cuts as shown in Figures 11, A and B, and 12, A to D.

CONCLUSION

In human otoconia, calcite nanocrystals together with the organic minority component are organized to form different arrangements of nanocomposite structures. There are 2 different volume densities within the uniform outer

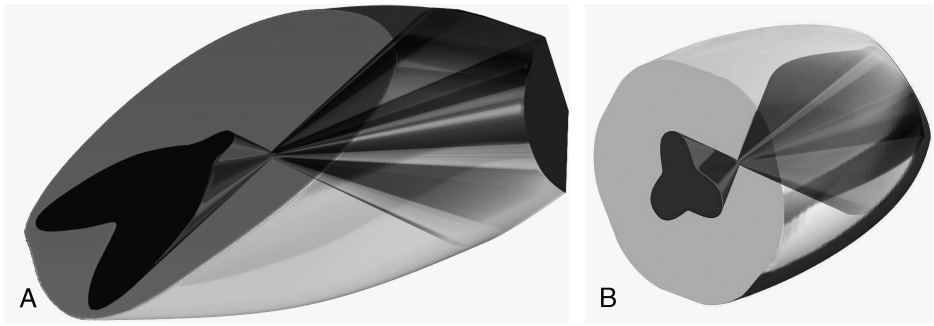

FIG. 11. *A* and *B*, The inner architecture of human otoconia consisting of branch and belly regions leads to various surface impressions depending on the direction of cuts and scratches, respectively. This is shown by the 3D model of human otoconia: Cut with a wing-like structure of the branches *A* and paramedian crosswise cut resembling a 3-leaf clover (*B*).

shape leading to an inner architecture consisting of 3 + 3 dense branches and a less dense belly region.

The degeneration of otoconia shows a gradual dissolution of the less dense belly area, whereas the branches are affected only in later stages. The center of symmetry of otoconia is the preferred site for fragment formation. Artificial otoconia are closely related to human otoconia and provide a suitable model system for further investigations.

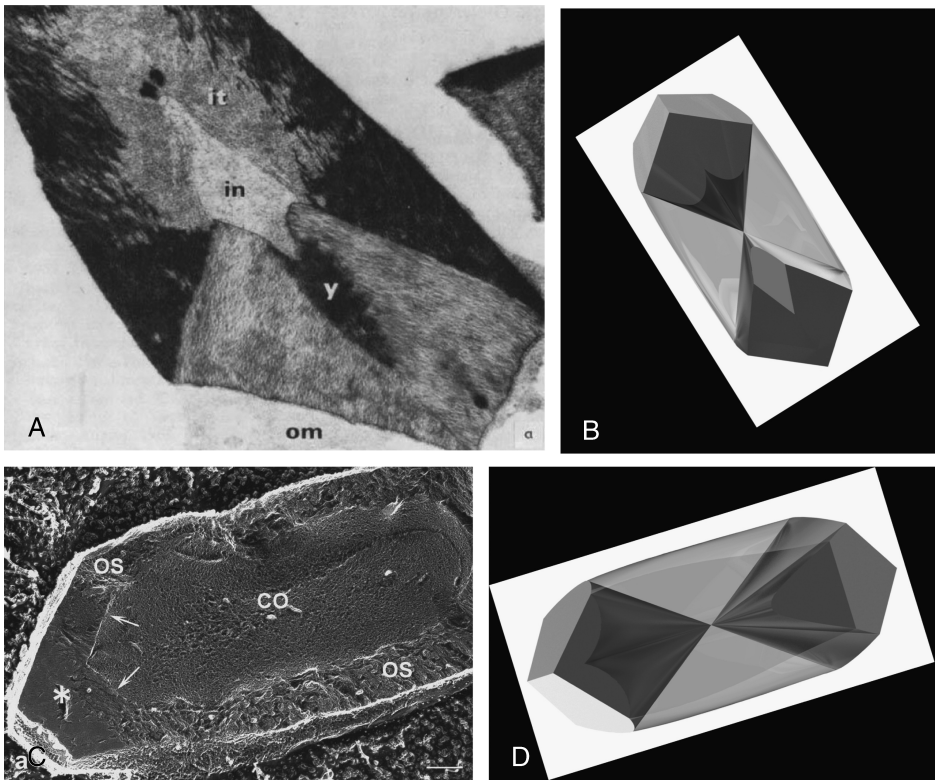

FIG. 12. *A*, SEM-image of an otoconium (diamond knife cut) reported in literature (10) leading to the assumption of a core shell/structure. Reprinted from: Sánchez-Fernández JM, Marco J, Rivera-Pomar JM, Delgado RM. Electron diffraction studies on otolith organization in the macula utriculi of the guinea pig. *Acta Otolaryngol* 1972;73:267–9, copyright 1972, Informa Healthcare. Reproduced with permission of Informa Healthcare. *B*, Belly/branch-model with approximate orientation as (*A*). The description ''y'' in (*A*) corresponds to a part of a branch or a part of a belly region adjoining 2 other branches revealing more ordered structures of fibrils. The description ''in'' and ''it'' in (*A*) also correspond to parts of branches surrounded by the belly (black). *C*, SEM-image of a fractured otoconium (Balzers 301 freeze-fracture apparatus) leading to the assumption of a core/shell structure. Reprinted from: Lins U, Farina M, Kurc M, Riordan G, Thalmann R, Thalmann I, Kachar B. The otoconia of the guinea pig utricle: internal structure, surface exposure, and interactions with the filament matrix. *J Struct Biol* 2000;131:1; 67–78, Copyright 2000, with permission from Elsevier. *D,* Belly/branch model with approximate orientation as (*C*). ''OS'' in (*C*) corresponds to parts of the belly area (bottom and top) as well as to parts of branches (left). The *arrows* indicate ordered fibrils belonging to part of branches. ''CO'' in (*C*) represents part of the belly area. The cuts in (*A*) and (*C*) appear oblique and the corresponding surfaces are not planar including artifacts due tothe cutting procedure (*asterisk*, ''knife marks on the surface'').

REFERENCES

1. Lindeman HH. Anatomy of the otolith organs. *Adv Otorhinolaryngol* 1973;20:405–33.
2. Merfeld D, Park S, Gianna-Poulin C, et al. Vestibular perception and action employ qualitatively different mechanisms. I. Frequency response of VOR and perceptual responses during translation and tilt. *J Neurophysiol* 2005;94:186–98.
3. Carlström D, Engström H. The ultrastructure of statoconia. *Acta Otolaryngol* 1955;45:14–8.
4. Carlström D, Engström H, Hjorth S. Electron microscopic and X-ray diffraction studies of statoconia. *Laryngoscope* 1953;63: 1052–7.
5. Ross MD, Peacor D, Johnsson LG, Allard LF. Observations on normal and degenerating human otoconia. *Ann Otol Rhinol Laryngol* 1976; 85:310–26.
6. Lim DJ. Otoconia in health and disease. A review. *Ann Otol Rhinol Laryngol Suppl* 1984;112:17–24.
7. Ross MD, Pote KG. Some properties of otoconia. *Philos Trans R Soc Lond B Biol Sci* 1984;13:445–52.
8. Fermin CD. High resolution and image processing of otoconia matrix. *Microsc Res Tech* 1993;25:297–303.
9. Marco J, Sánchez-Fernández JM, Rivera-Pomar JM. Ultrastructure of the otoliths and otolithic membrane of the macula utriculi in the guinea pig. *Acta Otolaryngol* 1971;71:1–8.
10. Sánchez-Fernández JM, Marco J, Rivera-Pomar JM, Delgado RM. Electron diffraction studies on otolith organization in the macula utriculi of the guinea pig. *Acta Otolaryngol* 1972;73:267–9.
11. Lins U, Farina M, Kurc M, et al. The otoconia of the guinea pig utricle: internal structure, surface exposure, and interactions with the filament matrix. *J Struct Biol* 2000;131:67–78.
12. Thalmann R, Ignatova E, Kachar B, Ornitz DM, Thalmann I. Development and maintenance of otoconia: biochemical considerations. *Ann N Y Acad Sci* 2001;942:162–78.
13. Andrade LR, Lins U, Farina M, Kachar B, Thalmann R. Immunogold TEM of otoconin 90 and otolin - relevance to mineralization of otoconia, and pathogenesis of benign positional vertigo. *Hear Res* 2012;292:14–25.
14. Simon P, Carrillo-Cabrera W, Huang YX, et al. Structural Relationship between Calcite–Gelatine Composites and Biogenic (Human) Otoconia. *Eur J Inorg Chem* 2011;35:5370–7.
15. Huang YX, Buder J, Cardoso-Gil R, et al. Shape development and structure of a complex (otoconia-like?) calcite-gelatine composite. *Angew Chem Int Ed Engl* 2008;47:8280–4.
16. Jang YS, Hwang CH, Shin JY, Bae WY, Kim LS. Age-related changes on the morphology of the otoconia. *Laryngoscope* 2006;116: 996–1001.
17. Campos A, Cañizares FJ, Sánchez-Quevedo MC, Romero PJ. Otoconial degeneration in the aged utricle and saccule. *Adv Otorhinolaryngol* 1990;45:143–53.
18. Suzuki H, Ikeda K, Takasaka T. Age-related changes of the globular substance in the otoconial membrane of mice. *Laryngoscope* 1997;107:378–81.
19. Walther LE, Westhofen M. Presbyvertigo-aging of otoconia and vestibular sensory cells. *J Vestib Res* 2007;17:89–92.
20. Liu F, Willhammar T, Wang L, et al. SM-5 zeolite single crystals with b-axis-aligned mesoporous channels as an efficient catalyst for conversion of bulky organic molecules. *J Am Chem Soc* 2012;134: 4557–60.
21. Ross MD, Peacor D, Johnsson LG, et al. Observations on normal and degenerating human otoconia. *Ann Otol Rhinol Laryngol* 1976;85: 310–26.